The DOI for this manuscript is doi: 10.1175/JAS-D-15-0049.1

The final published version of this manuscript will replace the preliminary version at the above DOI once it is available.

If you would like to cite this EOR in a separate work, please use the following full citation:

Boos, W., A. Fedorov, and L. Muir, 2015: Convective self-aggregation and tropical cyclogenesis under the hypohydrostatic rescaling. J. Atmos. Sci. doi:10.1175/JAS-D-15-0049.1, in press.

Convective self-aggregation and tropical cyclogenesis under the hypohydrostatic rescaling

William R. Boos*, Alexey Fedorov and Les Muir

Department of Geology and Geophysics, Yale University, New Haven, Connecticut, USA

**Corresponding author address:* William R. Boos, Department of Geology and Geophysics, Yale University, PO Box 208109, New Haven, Connecticut, USA

E-mail: billboos@alum.mit.edu

ABSTRACT

The behavior of rotating and non-rotating aggregated convection is examined at various horizontal resolutions using the hypohydrostatic, or Reduced Acceleration in the VErtical (RAVE), rescaling. This modification of the equations of motion reduces the scale separation between convective and larger-scale motions, enabling the simultaneous and explicit representation of both types of flow in a single model without convective parameterization. Without the RAVE rescaling, a dry bias develops when simulations of non-rotating radiative-convective equilibrium are integrated at coarse resolution in domains large enough to permit convective self-aggregation. The rescaling reduces this dry bias, and here it is suggested that the rescaling moistens the troposphere by weakening the amplitude and slowing the group velocity of gravity waves, thus reducing the subsidence drying around aggregated convection. Separate simulations of rotating radiative-convective equilibrium exhibit tropical cyclogenesis; as horizontal resolution is coarsened without the rescaling, the resulting storms intensify more slowly and achieve lower peak intensities. At a given horizontal resolution, using RAVE increases peak storm intensity and reduces the time needed for tropical cyclogenesis, effects here suggested to be caused at least in part by the environmental moistening produced by RAVE. Consequently, the RAVE rescaling has the potential to improve simulations of tropical cyclones and other aggregated convection in models with horizontal resolutions of O(10-100 km).

1. Introduction

The representation of moist convection in numerical models of atmospheric flow is a problem that has stymied the scientific community for decades. Computing power is typically insufficient to provide the spatial resolutions needed to successfully simulate moist convective motions in model domains large enough to represent planetary scale flow. At the same time, poor understanding of the net effects of convective motions has prevented the development of unbiased approximations of the subgrid-scale effects of moist convection; some argue that this sort of parameterization may not even be possible (for a review see Arakawa 2004).

These issues are particularly vexing when attempting to represent organized convection having horizontal scales on the order of 1-100 km, such as occurs in mesoscale convective systems and tropical cyclones. Such circulations lie in the gap that is sometimes assumed to exist between convective motions with horizontal scales of 0.1 - 1 km and the "large-scale" motions that can be explicitly represented in global models with horizontal grid spacings on the order of 100 km. While individual occurrences of organized convection can be simulated at extremely fine resolutions because only short times and relatively small domains need to be represented, simulation of the global distribution of organized convection is hindered by limited model resolution and inadequate convective parameterization.

Study of the effect of climate change on the global distribution of tropical cyclones (TCs) has been especially limited by these issues. Explicit representation of the O(10 km)-diameter TC eyewall is impossible at typical global climate model resolutions, so even the latest generation of those models can only simulate "TC-like storms" (e.g. Camargo 2013; Merlis et al. 2013). Although the space-time distribution of these TC-like storms is similar to the distribution of observed TCs, the model storms are larger and weaker than observed TCs (e.g. Manabe et al. 1970; McBride 1984;

Vitart et al. 1997). Even when regional models of the western North Pacific and tropical Atlantic were integrated at the relatively fine horizontal resolution of 18 km, the most intense simulated storms would be classified in Saffir-Simpson category three (Knutson et al. 2007; Wu et al. 2014). The question of how the characteristics of the most intense TCs (i.e. categories four and five) vary with the global climate state thus cannot be answered directly by most global and even regional numerical models. Downscaling methodologies have been developed in attempts to bypass this problem, using grid-scale fields from coarse-resolution global models as inputs to statistical or dynamical simulations of individual TCs (e.g. Emanuel et al. 2008; Bender et al. 2010; Zhao and Held 2010; Fedorov et al. 2010; Villarini and Vecchi 2012; Knutson et al. 2013). However, it seems fair to say that explicit representation of the most intense category of TCs in a global model remains a much sought after goal of the atmospheric science community.

Previous studies as well as this work show that faithful representation of TC structure and intensity requires model horizontal resolutions on the order of 1 km. For example, Gentry and Lackmann (2010) found that storm intensity increased as horizontal grid spacing was reduced from 8 km to 1 km, and they suggested that horizontal resolutions of 2-3 km are needed to resolve the eyewall processes that are important for operational prediction. Other studies find a more ambiguous dependence of storm intensity on horizontal resolution for grid spacings in the range of 1-5 km, and suggest that subgrid-scale parameterizations are at least as important as resolution for such grid spacings (Fierro et al. 2009; Sun et al. 2013). But it seems clear that coarsening horizontal resolution beyond 5-10 km greatly reduces the peak intensity achievable in simulated tropical cyclones: Murakami and Sugi (2010) found that 20-km grid spacing produced a large underestimate in the number of storms with intensities higher than Saffir-Simpson category 2. Peak storm intensity generally decreases as horizontal resolution is further coarsened past 10-20 km, so that typical global climate models, even at "high" resolutions of 25 or 50 km, do not simulate tropical cyclones with intensities greater than category 2 or 3 (Walsh et al. 2013; Strachan et al. 2013). This conclusion is confirmed by various simulations with global and regional atmospheric models (Zhao et al. 2009; Knutson et al. 2008, 2013) and coupled global climate models (e.g. Gualdi et al. 2008; Scoccimarro et al. 2011; Bell et al. 2013). A few global atmospheric models do produce TCs of higher intensity at 25-km resolution (e.g. Zarzycki and Jablonowski 2014), but this seems to depend on specifics of the convective parameterization used. The frequency and intensity of TCs simulated by global models with O(25-50 km) horizontal resolution is highly sensitive, sometimes in nonmonotonic and counterintuitive ways, to parameterizations of subgrid-scale physics and to the numerical damping used to suppress grid-scale noise (Zhao et al. 2012).

A new approach to the representation of moist convection in numerical models, proposed by Kuang et al. (2005, hereafter KBB), modifies the equations of motion to reduce the scale separation between convective and large-scale motions and thus allows explicit representation of both in the same model. This approach can be implemented and interpreted in multiple ways, but perhaps the simplest involves reducing the vertical acceleration of fluid parcels by introducing a factor $\gamma > 1$ in the vertical momentum equation,

$$\gamma^2 \frac{Dw}{Dt} = -\frac{1}{\rho}\frac{\partial p}{\partial z} - g + F_z. \qquad (1)$$

Here D/Dt is the material derivative, F_z is the vertical acceleration due to diffusion or other processes (typically acting on the subgrid scale), and other symbols have their usual meteorological meanings. This implementation, which KBB called Reduced Acceleration in the VErtical (RAVE), reduces the vertical velocities and increases the horizontal length scales of smaller convective motions, making them closer in size to those of the unaltered large-scale, hydrostatic flow. RAVE has also been referred to as the hypohydrostatic rescaling because it artificially increases the inertia of vertical motions (Pauluis et al. 2006; Garner et al. 2007). Although the RAVE/hypohydrostatic approach has received new attention in the past decade for its effects on moist convection, the same modification of the vertical momentum equation was used years earlier in so-called quasi-nonhydrostatic (QNH) models used for numerical weather prediction (MacDonald et al. 2000a; Lee and MacDonald 2000; Browning and Kreiss 1986; Skamarock and Klemp 1994). These QNH models were shown to be more numerically stable and resistant to small-scale error growth when subjected to impulsive forcings such as moist convective heating or initialization with an out-of-balance state. MacDonald et al. (2000b) showed that using (1) for the vertical momentum equation suppressed gravity wave generation below a certain length scale, thus slowing the adjustment to geostrophic or gradient wind balance while leaving Rossby waves and the large-scale response to diabatic heating unchanged.

As discussed by KBB, the RAVE rescaling is equivalent to the Diabatic Acceleration and Rescaling (DARE) approach, in which the planetary rotation rate is increased by a factor of γ, the planetary radius is decreased by γ, and diabatic processes such as radiative and surface enthalpy fluxes are increased by γ. The DARE approach shrinks the time and space scales of the large-scale dynamics (e.g. the Rossby deformation radius), bringing them closer to the scales of convective motions. Yet another mathematically equivalent approach is known as the Deep Earth rescaling, in which the gravitational acceleration is decreased and the vertical coordinate (z) is increased in scale by the factor γ (Pauluis et al. 2006). Although all of these treatments are mathematically identical, here we use the RAVE approach because it has perhaps the simplest physical interpretation and is easily implemented in numerical models. For more background and history on RAVE and equivalent rescalings, see KBB, Pauluis et al. (2006), and references therein.

RAVE and equivalent rescalings have been used to study a number of phenomena involving moist convection, but to our knowledge have not been used for studying TCs or tropical cyclogenesis. KBB presented preliminary results from an equatorial beta-plane simulation of the tropospheric general circulation forced by an equatorial sea surface temperature (SST) maximum, with some emphasis on the spectrum of convectively coupled equatorial waves. Garner et al. (2007) conducted global aquaplanet simulations with large RAVE factors (i.e. $\gamma \geq 100$) and found that the extratropical circulation was largely unaltered by use of even these extreme rescalings; they noted that use of RAVE with $\gamma \sim 3$ and horizontal resolutions on the order of 10 km may provide a promising alternative to convective parameterization. Boos and Kuang (2010) used RAVE in an equatorial beta-plane model to examine the mechanisms involved in tropical intraseasonal variability during boreal summer, with horizontal resolutions of about 30 km and $\gamma = 15$. Ma et al. (2014) examined the influence of topography on the South Asian monsoon using RAVE in a global model (on a sphere) without convective parameterization, at a horizontal resolution of 40 km with $\gamma = 10$.

The use of RAVE was criticized by Pauluis et al. (2006), who argued that for the same computational cost, coarse-resolution integrations without convective parameterizations more accurately reproduced the statistics of deep moist convection than integrations with RAVE. They based this argument on simulations of radiative-convective equilibrium in doubly-periodic domains in which the horizontal grid spacing was varied while the number of model grid points was held constant (thus larger domains were used at coarser resolutions). They simulated a 16 day period and analyzed the last 8 days, and found that tropospheric specific humidity decreased as resolution was coarsened and that RAVE enhanced the amplitude of this dry bias. In contrast, here we conduct much longer integrations holding domain size constant, and find that instead of enhancing a dry bias, RAVE actually reduces the dry bias caused by use of coarse resolution in simulations of radiative-convective equilibrium. We attribute this contrasting result to our use of a fixed domain size and longer simulation, and provide a more detailed comparison with the results of Pauluis et al. (2006) in an appendix.

The main goal of this paper is to examine the effects of RAVE on convective self-aggregation, both with and without rotation, in doubly periodic domains large enough to contain one TC. We present possible mechanisms by which RAVE influences the humidity field in radiative-convective equilibrium and in tropical cyclogenesis. This work is in some ways a methodological study showing that RAVE can compensate for some of the deleterious effects of coarse resolution on simulated TC intensity. But it also provides a closer look at the ways in which RAVE alters the interaction of organized moist convection with its environment. In particular, we apply some of the ideas of MacDonald et al. (2000b) for the effect of RAVE on the internal wave field to the topic of moist convection and the spatial distribution of moisture.

The next section of this paper presents details of the numerical model used in this work. Subsequent sections show results from simulations in doubly periodic domains, both with and without rotation. The paper ends with a summary and discussion of the method's possible value for future studies of TCs and aggregated convection.

2. Model details

This study uses the System for Atmospheric Modeling (SAM) version 6.3 by Khairoutdinov and Randall (2003), which integrates the anelastic equations of motion in Cartesian coordinates. The model has prognostic equations for liquid/ice water moist static energy, total precipitating water, and total nonprecipitating water. A five-class bulk microphysics scheme diagnoses rain, snow, graupel, cloud water, and ice. Numerous studies of radiative-convective equilibrium states have used this model, including some examinations of convective self-aggregation and spontaneous TC genesis (e.g. Bretherton et al. 2005; Muller and Held 2012).

We conducted integrations with and without rotation, all in domains of square, doubly periodic horizontal dimensionality. Integrations without rotation (i.e. $f = 0$) had domain widths of either

96 km, 384 km, or 768 km, referred to hereafter as the 1°-, 4°-, and 8°-wide domains, respectively. Integrations with rotation used domain widths of 1280 km and a Coriolis parameter equal to that found at 20°N on Earth. These domain widths may inhibit the size of simulated TCs and artificially confine the gravity waves that propagate away from organized convection. Indeed, Chavas and Emanuel (2014) found that the size of a simulated axisymmetric TC increased with domain size until the diameter of the domain was approximately 6000 km. Unfortunately, computational limits prevented use of larger domains in this work. Nevertheless, our chosen domain width of 1280 km is larger than that used in most previous studies of convective aggregation and spontaneous TC genesis (e.g. Bretherton et al. 2005; Muller and Held 2012; Wing and Emanuel 2013). Also, since individual occurrences of aggregated convection do not exist in isolation in the real world, use of larger idealized domains may not better represent reality.

All integrations used 64 vertical levels with vertical grid spacing ranging from 80 m near the surface to 400 m in the bulk of the troposphere and 1.2 km near the rigid lid at 27 km. To reduce gravity wave reflection and resonance, Newtonian damping was applied to wind, temperature, and water vapor in the top 30 percent of the domain with a time scale that decayed linearly from 2 minutes at the top to 2 hours at the bottom of this sponge layer. Time steps ranged from 4 to 50 seconds, depending on model resolution, with SAM automatically halving the time step when high Courant numbers were achieved.

All integrations used an oceanic lower boundary condition with an SST of 301 K and wind-dependent surface sensible and latent heat fluxes computed using a bulk surface flux formula with a prescribed minimum surface wind speed of 1 m s^{-1}. Fully interactive radiation was represented using parameterizations from the National Center for Atmospheric Research (NCAR) Community Climate Model (CCM) version 3.5 (Kiehl et al. 1998) with radiative fluxes calculated about once every 15 minutes. Insolation was set to its perpetual, diurnal mean equinox value at the equator for the nonrotating runs and at 20°N for the rotating runs. Ocean surface albedo depends on solar zenith angle and is about 0.08 for these integrations. Note that although use of interactive radiation does not alter the SST, moisture-dependent radiation has been shown to be essential for achieving self-aggregation of convection in SAM (Bretherton et al. 2005; Wing and Emanuel 2013; Emanuel et al. 2013). All integrations were initialized using a horizontally homogeneous tropical mean sounding, and symmetry was broken by adding white noise to the dry static energy field in the lowest five model levels with amplitude decreasing from 0.1 K at the lowest level to 0.02 K at the fifth level. Simulations with rotation were initialized using a moister mean sounding for reasons discussed below.

The RAVE rescaling was used in many integrations, with values of γ ranging from 1 to 16 (γ = 1 represents no rescaling). A Smagorinsky-type closure was used to represent subgrid-scale turbulence, with the parameterized stresses scaled by γ to account for the fact that RAVE alters the aspect ratio of the resolved eddies (see discussion in appendix of Pauluis et al. 2006). We did not directly modify microphysical processes when RAVE was used in our simulations, consistent with the methodology used in Pauluis et al. (2006). In particular, we did not scale the terminal velocity of falling condensate by γ.

3. Results for non-rotating domains

We first present results illustrating the effects of horizontal resolution and RAVE rescaling on non-rotating radiative-convective equilibrium. For domains larger than a few hundred kilometers in width, moist convection evolves over tens of days to an aggregated state consisting of a moist precipitating cluster surrounded by a dry nonconvecting region, as in our simulations conducted in 8°-wide domains (Figs. 1b, c). This self-aggregation of moist convection has been explored in detail in previous studies, and has been shown to require a minimum domain size of about 200 km and to be caused by feedbacks between tropospheric moisture and radiation (e.g. Muller and Held 2012; Wing and Emanuel 2013). Consistent with those studies, we find that the smallest domain (1° wide) has convective activity and a moisture field that is horizontally homogeneous in the time mean (Fig. 1a).

Models integrated at coarser resolutions undergo convective aggregation more quickly and have lower domain-mean moisture content than integrations conducted at finer resolutions. This can be seen in the instantaneous distribution of precipitable water (PW) 50 days after model initialization, which has a drier and more horizontally extensive non-convecting region in the integration conducted at 16 km horizontal resolution than in the standard 2 km-resolution run (Fig. 1c). The 16 km-resolution integration also took about half the time to aggregate as the 2 km-resolution integration (Fig. 2). While the dependence of aggregation time on horizontal resolution is generally monotonic in the integrations shown here and in others not shown, the dependence of domain-mean PW on horizontal resolution is less regular. For instance, an integration conducted at 8 km resolution exhibits nearly the same equilibrium PW as the 2 km run, although oscillations in the PW field in both runs make comparison difficult. Similar oscillations in the PW field were seen in some of the simulations of Bretherton et al. (2005, their Fig. 5a), and are associated with variations in the size of the moist region. But in general, coarser resolutions typically produce a drier domain. The 16 km-resolution integration equilibrates with a domain mean PW several mm lower than that of the 2 km-resolution integration. This general pattern can be seen in vertical profiles of specific humidity in this 8°-wide domain and in a 4°-wide domain (Fig. 3). Coarse resolution runs also typically have a colder troposphere and a warmer stratosphere than fine resolution runs. The dry bias may cause at least some of the temperature bias, because one expects a tropospheric cooling and stratospheric warming as the longwave emissivity of the column decreases. However, the warmer stratosphere is also consistent with a simple reduction in the height of the tropopause, as occurs during a tropospheric cooling, combined with an unchanged stratospheric lapse rate.

Use of the RAVE rescaling generally produces a moister equilibrium state. The dry bias seen in the equilibrium state of runs using the 4°-wide domain at 12 km resolution is nearly eliminated when a rescaling factor of $\gamma = 3$ is used at the same horizontal resolution (Fig. 4a); there is a moist bias near the surface and a weak dry bias above that nearly cancel in a vertical integral. Increasing γ to 6 produces a moist bias that is roughly the same amplitude as the original dry bias (as a reminder, all biases are assessed relative to integrations using the same domain size at 2 km resolution with $\gamma = 1$). A further increase of γ to 12 produces a humidity profile that looks more like that obtained for $\gamma = 3$. This nonmonotonic dependence of the moisture field on γ is associated with the system transitioning to a non-aggregated state after roughly 120 days of model time for $\gamma = 6$ but not for the larger value of $\gamma = 12$. Given that the combination of a domain size of 4° and an SST of 301 K lies near a threshold in the parameter space for self-aggregation (e.g. Wing and Emanuel 2013; Muller and Held 2012), it is perhaps not surprising that some combinations of parameters produce runs that occasionally slip into a moister, non-aggregated state. These transitions back to a non-aggregated state do not occur in any simulations we conducted using the larger domain width of 8°. For example, for integrations with 16 km resolution and an 8°-wide domain, increasing γ from 1 to 8 and then to 16 produced a monotonic moistening of the troposphere (Fig. 4c). The RAVE rescaling also produces a temperature bias that is of similar magnitude but opposite sign to that seen in coarse resolution runs without the rescaling: RAVE creates a warm bias in the lower to middle troposphere and a cold bias in the upper troposphere and lower stratosphere.

In summary, coarse resolution integrations without RAVE (i.e. $\gamma = 1$) produce a troposphere that is too dry and too cold compared to fine resolution simulations. Convective self-aggregation also occurs too quickly in coarse resolution simulations. When coarse resolution models are integrated with moderate values of γ, the dry bias is reduced to give PW values near those seen in the fine resolution control runs, although RAVE does typically produce an overly strong moistening of the near-surface air together with a more moderate reduction of the dry bias at higher altitudes. Previous studies (e.g. Pauluis et al. 2006) arguing that RAVE does not reduce and may even amplify the dry bias seen in coarse resolution runs may have failed to account for the aggregation of convection that occurs as domain size is increased. In an appendix we present additional model integrations that allow for better comparison with that previous work.

4. A hypothesis for the effect of RAVE on aggregated convection

We now present a mechanism that may explain how RAVE moistens the troposphere in simulations of radiative-convective equilibrium. Previous arguments for the influence of RAVE on the moisture field have taken a local view in which RAVE slows convective overturnings, with these overturnings directly influencing the moisture field through vertical advection (e.g. Pauluis et al. 2006). However, such arguments are relevant only to regions in which convection is active, and when convection has aggregated the domain-mean humidity is dominated by values in the non-convecting region. The key issue, then, is how RAVE alters humidity in the non-convecting region outside a convective cluster.

Locations outside of active convection (but within a deformation radius) are known to have temperatures set by spreading gravity wave-like disturbances that produce net subsidence and adiabatic warming as they pass (e.g. Bretherton and Smolarkiewicz 1989; Nicholls et al. 1991; Mapes 1993; Cohen and Craig 2004). The subsidence produced by these buoyancy bores also dries areas around the convecting region by advecting dry air downward from the upper troposphere. At the same time, shallower and slower-moving buoyancy bores have been argued to lift and destabilize the environment near the original convection. Thus, while properties of the convecting region might be set primarily by the convective motions themselves, properties of the environment around an actively convecting region are controlled indirectly via the gravity waves that emanate from the convection. Here we discuss how the modification of the internal wave field by RAVE, which was studied by MacDonald et al. (2000b) in the context of numerical weather prediction, might alter humidity and subsequent convection around a convecting cluster.

Skamarock and Klemp (1994) showed that RAVE modifies the dispersion relation for linear, Boussinesq, nonhydrostatic gravity waves to be

$$\nu^2 = \frac{f^2 m^2 + N^2 k^2}{\gamma^2 k^2 + m^2}, \tag{2}$$

where m is the vertical wavenumber, k is the total horizontal wavenumber, and ν is frequency. Anticipating results that will be presented in the next section, we have included rotation using an f-plane approximation. The horizontal phase speed and group velocity are, respectively,

$$c_x = \frac{N}{\sqrt{\gamma^2 k^2 + m^2}} \sqrt{1 + \frac{f^2 m^2}{N^2 k^2}} \tag{3}$$

$$c_{gx} = \frac{m^2 \left(N - \frac{f^2 \gamma^2}{N} \right)}{(\gamma^2 k^2 + m^2)^{\frac{3}{2}} \sqrt{1 + \frac{f^2 m^2}{N^2 k^2}}}. \tag{4}$$

The use of RAVE thus decreases both the horizontal phase speed and group velocity of gravity waves. If $\gamma \lesssim 10$, then $f\gamma << N$ for typical atmospheric values of f and N, and the group velocity is well approximated by

$$c_{gx} \simeq \frac{N m^2}{(\gamma^2 k^2 + m^2)^{\frac{3}{2}} \sqrt{1 + \frac{f^2 m^2}{N^2 k^2}}}. \tag{5}$$

The coefficient by which RAVE reduces the group velocity is then

$$\frac{c_{gx,RAVE}}{c_{gx}} = \left(\frac{k^2 + m^2}{\gamma^2 k^2 + m^2} \right)^{3/2} \tag{6}$$

which is valid without the assumption of hydrostatic balance. This ratio is plotted in Fig. 5a for a vertical wavelength of 28 km, $N = 0.01\ \mathrm{s}^{-1}$, and f at 30° latitude. These results are consistent with the frequency response found by MacDonald et al. (2000b), but here we focus on wave speeds to better connect with previous work showing that these wave speeds set the rate at which subsidence warming spreads away from a pulse of convection (e.g. Bretherton and Smolarkiewicz 1989; Mapes 1993; Cohen and Craig 2004). MacDonald et al. (2000b) also showed that the amplitude of the vertical velocity response to an initial temperature perturbation or a heating impulse is proportional to the frequency ν and so is also reduced by RAVE. For this reason we also plot the ratio by which RAVE reduces the frequency, ν_{RAVE}/ν, in Fig. 6.

As expected, the use of RAVE has the largest effect on nonhydrostatic waves (i.e. those with horizontal wavelengths shorter than 100 km), for which the group velocity scales like γ^{-3} and the amplitude scales like γ^{-1}. But RAVE also substantially reduces the horizontal group velocity and amplitude of longer waves for which the hydrostatic dispersion relation would, without RAVE, be a good approximation. For example, the group velocity and frequency (which is proportional to amplitude) are reduced to about 60% and 80% of their standard values, respectively, for a horizontal wavelength of 200 km and the moderate value of $\gamma = 5$. RAVE alters c_{gx} and ν less for higher vertical wavenumbers, which is illustrated by evaluating (6) and (2) for a vertical wavelength of 14 km (Figs. 5b and 6b).

Our core argument is that RAVE slows the geostrophic adjustment process that returns the environment around episodic convective heating to a balanced state, and this slower adjustment process includes weaker subsidence that produces less vertical advective drying of the environment. The slowing of the geostrophic adjustment process is accomplished through a reduction in the horizontal speed and amplitude of inertia-gravity waves, and this reduction acts more strongly on waves with longer vertical wavelengths and shorter horizontal wavelengths, as detailed by previous authors (Skamarock and Klemp 1994; MacDonald et al. 2000b) and discussed above. In particular, the deeper waves that suppress remote convection are more strongly slowed and weakened by RAVE, which will reduce static stability and subsidence drying far from the original convection and enhance static stability and drying near the convection. The shallow internal waves hypothesized to be responsible for initiating convection via low-level lifting adjacent to an initial convective disturbance (e.g. Mapes 1993) are less affected by RAVE, so they can continue to propagate into and initiate convection in the far field. All of these effects act to encourage future convection in the far-field environment and to suppress it near the original convection, reducing the horizontal variance of humidity and convection in the domain.

This is analogous to the "rotational trapping" of gravity waves, which Liu and Moncrieff (2004) argued makes convective clustering less likely at higher magnitudes of the Coriolis parameter (see also Bretherton et al. 2005). One notable difference is that rotation provides an inherent length scale in the Rossby deformation radius, while RAVE alters the rate at which the geostrophic adjustment occurs. Given a sufficiently long time after an episode of convective heating, RAVE would thus make little to no difference in the final adjusted state. However, we are working with a radiative-convective equilibrium state that is constantly destabilized by radiative cooling and surface heat fluxes, and so hypothesize that reducing the rate at which the environment around a convecting cluster warms will foster convection in that environment by reducing its static stability. We also hypothesize that reducing the rate of subsidence drying will result in a moister environment because that environment is constantly moistened by eddy fluxes of moisture, perhaps mostly due to vertical transports by shallow convective motions.

One caveat is that the convective heating that initiates any geostrophic adjustment is itself affected by RAVE in ways that may modify the above arguments. RAVE increases the horizontal scale of convective updrafts, and so the modified convection may excite longer wavelengths of gravity waves. This would compensate for the reduction in wave speed that occurs at a given wavelength because, in the absence of rotation, the transformation $k \to k/\gamma$ results in $c_{gx,RAVE} \to c_{gx}$ (with rotation, the group velocity still decreases as γ increases, but the functional form is different and this would not be relevant to our results in non-rotating domains). However, the frequency, and thus the amplitude, of the wave response continues to scale like γ^{-1} under this transformation:

$$\nu^2 \to \frac{N^2 k^2}{\gamma^2 (k^2 + m^2)} \tag{7}$$

where we have again neglected rotation. So even if the broadening of convective updrafts by RAVE resulted in no net change in the group velocity of the convectively excited gravity waves, we would still expect a reduction in wave amplitude. Nevertheless, it is important to emphasize that many of the above arguments neglect potentially important feedbacks. One of these is the radiative feedback of the modified humidity field, which one might expect to counter some of the effect of RAVE on the environmental temperature field (e.g. less subsidence warming and drying produces a moister atmosphere that cools less efficiently via radiation, albeit with some dependence on the vertical moisture profile). This is one reason why we have not attempted to argue that the effects of RAVE should be apparent in the time-mean temperature field. Furthermore, any simple horizontal average of temperature (such as that presented in Fig. 4) would by construction include the near-field increase and far-field decrease in static stability hypothesized to be induced by RAVE.

Another possibility is that RAVE may influence shallow convective motions that moisten the lower troposphere. RAVE is expected to increase the horizontal scale of convective motions in general, which might allow shallow convection to be better resolved at a given horizontal resolution. Pauluis and Garner (2006) attributed the dry bias that occurs in coarse-resolution models of radiative-convective equilibrium to the inability of those simulations to represent the vertical mixing caused by shallow clouds. While shallow turbulence occurs on sub-kilometer length scales that cannot be resolved at any of the grid spacings used here, substantial vertical mixing is also generated by cold pools with length scales of a few to tens of kilometers (Moeng et al. 2009). We find that the variance of eddy vertical velocity at 1 km altitude decreases greatly as resolution is coarsened in our 8°-wide domain (Fig. 7). The enhanced variance that occurs for grid spacings finer than 16 km occurs entirely on length scales smaller than 16 km, as indicated by the fact that there is no change in variance as a function of resolution when w is block-averaged to 16×16 km before calculating its eddy variance. But the more salient point is that RAVE does not increase the variance of eddy vertical velocity as γ is increased from 1 to 16 at 16-km resolution. So these results are consistent with the idea that vertical mixing by shallow convection is inhibited at coarse resolutions, but they do not support the idea that RAVE moistens the troposphere by amplifying shallow overturnings.

5. Results for rotating domains

a. Effect of resolution

We now examine the spontaneous cyclogenesis that occurs in simulations of radiative-convective equilibrium in rotating domains. Emanuel and Nolan (2004) and Bretherton et al. (2005) showed that when simulations of radiative-convective equilibrium are performed on an f-plane, convection self-aggregates and evolves into a TC. This behavior is reproduced in our simulations using domains 1280 km wide with the Coriolis parameter equal to that at 20°N. When these simulations were conducted at 1 km horizontal resolution, cyclogenesis took roughly 30 days to occur and the simulated TC occupied about half the domain with a drier, non-convecting region occupying the other half (Figs. 8a, 9a). Integrations conducted at the coarser horizontal resolutions of 5 and 8 km took considerably longer — typically 40 to 50 days — to undergo cyclogenesis. There is a fair amount of variability in the time needed for cyclogenesis at a particular resolution; these integrations were initialized with small-amplitude random noise in the low-level dry static energy field, and small ensembles of integrations (4 ensemble members at each resolution) reveal that the time needed to produce a category 1 TC can vary by tens of days at a given resolution. But there is a clear delay of cyclogenesis as resolution is coarsened from 1 to 5 and then to 8 km (Fig. 10a). As resolution is further coarsened to 16 km, the time needed to achieve category 1 intensity actually decreases, but the cyclone only barely achieves that intensity and the intensification process lacks the abrupt character seen in the fine-resolution runs. Zhao et al. (2012) found that the frequency of TC genesis changed nonmonotonically as a horizontal cumulus mixing rate in a GCM was increased, although it is unclear whether this has any relation to the resolution-dependence illustrated here.

The delay of cyclogenesis at coarser resolutions contrasts sharply with the effect of resolution on self-aggregation time in non-rotating domains, where coarser resolutions produced faster aggregation (e.g. Fig. 2). Indeed, convective self-aggregation and tropical cyclogenesis seem to be two separate processes that take place on different time scales. To better illustrate this, we initialized all rotating simulations (including those discussed above) with a moister sounding having precipitable water of over 50 mm (integrations without rotation were initialized with a sounding having PW of about 37 mm). Use of this moister sounding does not qualitatively change any of the results presented here, as was confirmed by repeating all runs with the drier initial sounding, but allows for better illustration of the initial convective self-aggregation. Fig. 8b shows that the initial decrease of PW occurs more rapidly at coarser resolutions, as it did in the non-rotating simulations. This domain-mean drying accompanies the convective self-aggregation process, as illustrated in the previous section and discussed by Bretherton et al. (2005), and indicates that the time needed for self-aggregation decreases monotonically as resolution is coarsened. The faster aggregation at coarser resolutions is consistent with the larger peak surface wind speeds achieved at coarser resolutions in the first 15 days of model time (Fig. 8a). At 1 km resolution, the self-aggregation time scale is similar to the time needed for cyclogenesis, so that it seems like the two might occur simultaneously as part of a single process. But at resolutions of 5 and 8 km, only about 20 days is needed to form a single moist cluster surrounded by a dry region, while about 30 additional days are needed for this cluster to undergo intensification to a category 1 TC. Once peak surface wind speeds of almost 20 m s^{-1} are achieved (i.e. tropical storm intensity), the increase to peak intensity occurs quite rapidly — within about 5 days — and has greater rapidity at finer resolutions. The PW and surface wind speeds thus suggest the existence of multiple time scales: a 20-day time scale associated with the initial convective aggregation and domain-mean drying, a subsequent 10-40 day time scale associated with the formation of a tropical storm, and a 5-day time scale of rapid intensification of the storm to hurricane strength (these particular numbers might vary for different basin sizes, initial soundings, etc.). This is consistent with the idea that a "preconditioning" period exists prior to TC genesis, during which there is a moistening and cooling of the lower troposphere (Bister and Emanuel 1997) and/or diabatic production of low-level potential vorticity anomalies (Hendricks et al. 2004).

The peak intensity achieved by TCs decreased as resolution was coarsened. As the horizontal grid spacing of the rotating simulations was increased from 1 to 16 km, the peak intensity fell monotonically from Saffir-Simpson category 5 to category 1 (Figs. 8a and 10). The peak intensity achieved for each horizontal resolution exhibited less variability among ensemble members than did the time needed to reach category 1 intensity. These results are consistent with the propensity for coarse resolution regional models to simulate TCs with an intensity distribution that peaks at category 2-3 (e.g. Wu et al. 2014), and for global models with O(100 km) horizontal grid spacing to simulate only "TC-like" vortices. More generally, the peak intensity of simulated TCs has been shown to decrease as model horizontal resolution is coarsened, although most studies of this effect have used realistic initial and boundary conditions to simulate an observed TC. Gentry and Lackmann (2010) and Sun et al. (2013) found that peak intensity was reduced as grid spacing increased from 1 to 8 km in simulations of Hurricane Ivan (2004) and Typhoon Shanshan (2006), respectively. Fierro et al. (2009) found substantial changes in the simulated structure of Hurricane Rita (2005) as resolution was coarsened from 1 to 5 km, but little change in typical measures of storm intensity; further coarsening of resolution beyond 5 km did reduce peak intensity. All of these studies prescribed an initial vortex and did not note any strong effect of resolution on the time needed for TC intensification.

Here we suggest that TC intensity is limited and cyclogenesis delayed at coarse resolutions at least in part because coarse-resolution simulations produce a drier environment around the storm. Multiple studies have argued that a near-saturated troposphere is required for TC genesis (e.g. Emanuel 1989, 1995; Bister and Emanuel 1997; Frisius 2006; Raymond et al. 2007), so it seems plausible that a dry bias might inhibit the intensification of a TC in a model. We do not seek to determine whether the dry bias directly inhibits precipitating ascent in the TC eyewall or whether it acts indirectly by enhancing convective downdrafts outside the eyewall that cool and dry the subcloud layer; instead we simply invoke the general idea that TC genesis and intensity are inhibited in dry environments. The moisture field in our integrations with rotation was affected by resolution in a way qualitatively similar to that seen in the non-rotating integrations. During the first 20 days of integration, the time-mean, domain-mean PW decreased monotonically as resolution was coarsened from 1 to 16 km (Fig. 8b). On the day the TC achieved category 1 intensity, the environment around the storm was drier in integrations conducted at 8 km resolution than in those conducted at 1 km resolution (e.g. Fig. 9). The radial moisture gradient is enhanced even more at coarser resolutions when the TCs achieve category 2 intensity and the eyewall, as indicated by the surface wind speed distribution, is larger and somewhat more ragged at coarser resolutions (e.g. Fig. 11a, b).

To illustrate the resolution-dependence of the humidity field more quantitatively, we present horizontal distributions of 6-hour averages of PW during the first two days on which the storm had an intensity of category 1, with all model output coarsened via block averaging to the same 16 km grid. The mode of the horizontal distribution of PW clearly shifts to lower values at coarser resolutions (Fig. 12b). At the same time, the moist region (i.e. the eye and eyewall of the TC) became moister as resolution was coarsened, as evidenced by the upward shift in the upper tail of the PW distribution and by the example shown in Fig. 11.

These changes in humidity are accompanied by changes in the distribution of vertical velocities. Explicit simulations of convection are expected to produce slower ascending motions as horizontal resolution is coarsened beyond about 1 km because updrafts at these resolutions typically have a width of a single grid cell and thus a more shallow aspect ratio. Buoyant parcels with a shallow aspect ratio rise more slowly because they are closer to the hydrostatic limit in which the buoyancy-induced vertical pressure gradient force balances the buoyancy force itself. In contrast, for narrow parcels, the pressure gradient force facilitates ascent by horizontally diverging air above the parcel out of the parcel's upward path (e.g. Houze 1993). Slower ascent of individual parcels was documented in the simulations of Pauluis and Garner (2006), who derived a theoretical scaling for the dependence of updraft speed on model horizontal resolution. Slower ascent is seen at coarser resolutions in our rotating simulations (e.g. the left tail of the 500 hPa vertical velocity distributions in Fig. 12a), although this may represent organized ascent in the TC eyewall that is less directly controlled by the local vertical buoyancy force.

While previous studies have examined how updraft speed depends on horizontal resolution, less attention has been given to how resolution affects the subsiding motions that adiabatically warm and dry the environment around a precipitating cluster. In our simulations, downward velocities increase as resolution is coarsened, as evidenced by the distribution of vertical velocity at 500 hPa on the two days after the TCs achieved category 1 intensity (Fig. 12a).

Lane and Knievel (2005) examined the spectrum of gravity waves excited by a buoyancy anomaly that was 10 km wide in models with variable horizontal resolution, and found that coarser resolutions produced more power at longer wavelengths. Although they did not discuss the far-field subsidence, their figures show that the spreading gravity wave front travelled a greater distance after one hour of simulation at a resolution of 1.5 km than it did at the very fine resolution of 63 m. The group velocity of nonhydrostatic gravity waves increases with horizontal wavelength, as can be seen from (5), which for the nonrotating case without RAVE reduces to

$$c_{gx} \simeq \frac{Nm^2}{(k^2+m^2)^{\frac{3}{2}}}. \tag{8}$$

Although some discussions of the remote response to a convective cluster assumed a hydrostatic gravity wave field, for which $c_{gx} \simeq N/m$ (e.g. Mapes 1993), non-hydrostatic effects slow the group velocity to about 90% of its hydrostatic value for a horizontal wavelength of 100 km and to about 50% of its hydrostatic value for a wavelength of 40 km. Given that Lane and Knievel (2005) found a peak response at 10 km wavelength in the simulated spectrum of stratospheric gravity waves excited by idealized convection, these nonhydrostatic effects would seem to matter for determining the speed at which gravity wave pulses propagate away from a convecting region. Coarser horizontal resolutions would be expected to partition more energy into the longer-wavelength part of the gravity wave spectrum, and it is that part of the spectrum that has faster group velocities. It is unclear whether this faster spreading of gravity waves away from the precipitating cluster would result in stronger environmental subsidence. If radiative cooling balances subsidence warming in the time-mean, then an increase in the rate at which subsiding motions enter a region might result in stronger subsidence. But unlike the effects of RAVE, we have no theory to show that the amplitude of vertical velocities is influenced directly by horizontal resolution.

In summary, we suggest that coarser resolutions produce slower and wider updrafts together with a geostrophic adjustment process that is accomplished by gravity waves with longer horizontal wavelengths and thus faster group velocities. Our simulations produce stronger subsidence at coarser resolutions, as part of a more general reduction in skewness seen in the histograms of 500 hPa vertical motion. Whether this can be explained by the faster group velocity of gravity waves is unclear, and so the cause of the stronger subsidence at coarser resolutions is unclear. Vertical velocity distributions in the nonrotating simulations exhibit a similar sensitivity to horizontal resolution (not shown), which suggests that the resolution-dependence of the vertical velocity skewness arises from a mechanism that is general to aggregated convection and not one that involves, for example, TC eyewall dynamics.

b. Effect of RAVE

Since we showed that RAVE reduces the group velocity and amplitude of gravity waves and compensates for the dry bias seen in coarse-resolution simulations of convectively aggregated states, it seems natural to ask whether RAVE might reduce some of the bias seen in simulations of cyclogenesis at coarse resolutions. In our rotating simulations, the use of RAVE does produce a moister domain and decrease the time needed for TC genesis. Increasing γ from 1 to 8 in simulations with 8 km resolution reduces the time needed to achieve category 1 intensity from about 50 days to 15 days (Fig. 13). It also increases the peak surface wind speeds by 10 m s^{-1}or more, which corresponds to an increase of one to two Saffir-Simpson intensity categories.

At the time at which the storm first achieves category 1 intensity, RAVE produces a large increase in the domain-mean precipitable water, compensating for the dry bias seen in the coarse-resolution simulations without RAVE (Fig. 14, compare with Fig. 9). On the day the storm achieves category 2 intensity, the use of $\gamma = 4$ appears to have eliminated, and perhaps even slightly overcompensated for the biases in radial moisture gradient and eyewall size that arose from using the coarser resolution of 8 km (Fig. 11). The histogram of PW values narrows as γ is increased from 1 to 4 so that it becomes more like the PW histogram for the control simulation at 1 km resolution without RAVE; the bias in the histogram of vertical velocity is also reduced (Fig. 12c, d). Use of $\gamma = 8$ at 8 km resolution produces a domain that is too moist and results in genesis that occurs too quickly relative to the fine-resolution control run. Eyewall diameter also becomes smaller as γ is increased. Gentry and Lackmann (2010) found that the radius of maximum wind increased when horizontal grid spacing was increased in simulations of an observed hurricane, so this decrease in storm size might also be seen as correcting a bias caused by low resolution (though an over-correction clearly occurs for $\gamma = 8$).

At 16 km resolution, use of $\gamma = 16$ produces little change in the time needed to achieve category 1 intensity, but does allow the peak storm intensity to increase by a full Saffir-Simpson category (Fig. 13). These changes may be desirable from the perspective of bias reduction since the 16 km-resolution simulations with $\gamma = 1$ did not exhibit a delay in the time needed to achieve category 1 intensity but did exhibit overly weak storm intensities.

6. Summary and discussion

Using simulations of radiative-convective equilibrium in a cloud system-resolving model, we demonstrated that the environment around a precipitating cluster becomes drier as model resolution is coarsened from 1 km to O(10 km). This dry bias occurs at coarse resolutions in both rotating and non-rotating domains, and is accompanied by overly intense subsidence outside the moist cluster. In rotating domains, the convective cluster spontaneously evolves into a tropical cyclone, but this genesis is delayed and the peak TC intensity is reduced as model resolution is coarsened.

Many of these biases that occur at coarse resolutions can be compensated for by the RAVE rescaling: the dry bias is reduced, TC genesis occurs at earlier times, and the peak TC intensity is increased for $\gamma > 1$. We suggest that these effects of RAVE are caused at least in part by the influence of the rescaling on the domain-mean moisture field via a reduction in the amplitude and horizontal group velocity of gravity waves. Although this hypothesis may seem somewhat speculative at this stage because we have not provided any explicit evidence that the moisture field was altered by changes in gravity wave characteristics, it is a corollary of several existing ideas. Multiple previous studies have shown that the dry region outside a convective cluster is produced by subsidence created by the buoyancy bores that spread outward from the convective source (e.g. Bretherton and Smolarkiewicz 1989; Nicholls et al. 1991; Mapes 1993). Reducing the group velocity of these gravity wave packets by increasing the Coriolis parameter has been argued to trap subsidence closer to the convective source and thus to reduce the contrast in subsidence and humidity between the convective cluster and its far-field environment (Liu and Moncrieff 2004; Bretherton et al. 2005). Here we argue that a reduction in the amplitude and group velocity of gravity waves produced by RAVE should have an analogous effect on the distributions of vertical motion, humidity, and convection. Previous studies showed that RAVE slows the process of adjustment to a balanced state by altering the gravity wave dispersion relation (Skamarock and Klemp 1994; MacDonald et al. 2000b), but did not consider the implications for the distribution of humidity or subsequent moist convection. The idea that RAVE reduces the horizontal contrast in humidity by trapping buoyancy anomalies near an initial pulse of moist convection constitutes a new view of the manner in which RAVE influences organized convection. Prior work focused on how RAVE slows the vertical convective motions themselves (e.g. Kuang et al. 2005; Pauluis et al. 2006) rather than the slower subsiding motions that operate on the much larger length scale of a Rossby deformation radius.

The effects of RAVE on the group velocity of gravity waves may be desirable if the group velocity is biased high in coarse-resolution simulations of convection. While we have not demonstrated this definitively here, Lane and Knievel (2005) showed that the spectrum of gravity waves excited by convection is centered at longer wavelengths in simulations conducted at coarser resolutions, and longer waves do have a faster group velocity. Furthermore, RAVE reduces the bias in the horizontal distribution of mid-tropospheric vertical velocity that occurs in coarse-resolution simulations of TCs. It is thus possible that RAVE directly addresses the cause of the dry bias seen in coarse-resolution simulations, rather than introducing a moist bias by some mechanism independent of that which creates the original dry bias. Yet there is still much to explore here, and the effects of resolution and RAVE on the vertical moisture fluxes produced by shallow convection merit further examination.

The use of large RAVE factors can overcompensate for the biases seen in coarse-resolution simulations. While using $\gamma = 4$ at 8 km resolution produced PW distributions similar to those seen in the fine-resolution control run, using $\gamma = 8$ produced a domain that was too moist and TC genesis that occurred too soon. Similarly, the dry bias seen in 16 km-resolution simulations with $\gamma = 1$ was largely eliminated when γ was increased to 8, but became a moist bias at $\gamma = 16$. One would probably want to avoid using values of γ that are large enough to create a moist bias stronger than the original dry bias. Since the nature and magnitude of the biases created by use of coarse resolution likely depend on model numerics and grid, it may not be possible to provide a universal recommendation for the optimal value of γ. However, our results indicate that values of γ that would provide a resolution "equivalent" to that of the control run (e.g. $\gamma = 8$ at 8 km resolution for a control run at 1 km resolution) may be too high. This may be because it is more important to tune the gravity wave group velocity rather than some sort of effective resolution, and that group velocity scales like γ^{-3}.

While we have focused on the effects of resolution and RAVE on the ambient moisture field, the influence on organized convection might manifest via other mechanisms. For instance, resolution might limit peak TC intensity through its influence on the explicit representation of eyewall structure (e.g. Fierro et al. 2009; Gentry and Lackmann 2010). Or resolution might produce environmental drying through microphysical effects not explored here, such as less precipitation falling outside of saturated updrafts when those updrafts are wider at coarser resolutions, thereby increasing the precipitation efficiency. RAVE might enhance the intensity of TCs through the cooling effect it seemed to have in the upper troposphere and lower stratosphere (Emanuel 1988), but simple estimates suggest that this cooling should produce an increase in the maximum potential intensity of 1-2% for the RAVE numbers considered here. Given that coarse resolution integrations without RAVE can also have large temperature biases in the upper troposphere and lower stratosphere, it is not obvious that this effect of RAVE is any worse than the effect of integrating at coarse resolution or using parameterized convection. Another possibility is that RAVE might make a TC less sensitive to mid-tropospheric dry air by enhancing the horizontal scale of the precipitating upward mass flux in the eyewall and thereby reducing any drying by eddies that act diffusively, which is distinct from making ambient air less dry. Finally, it should be remembered that the limited domain size used in our simulations may influence TC size, TC intensity, and the rapidity of cyclogenesis in ways that depend on resolution or RAVE factor (e.g. Chavas and Emanuel 2014). Despite all these caveats, the environmental moisture field is thought to play an important role in TC genesis and intensification (e.g. Bister and Emanuel 1997; Frisius 2006; Raymond et al. 2007), and our results show that this field is influenced by resolution and RAVE.

Further assessment will be required before RAVE can be used routinely in operational or research models. However, this study shows that even without RAVE, numerical models with horizontal resolutions coarser than a few kilometers have large biases in the simulation of organized convection and its non-convecting environment. In deciding whether to use RAVE in numerical models of organized convection, one should remember that traditional convective parameterization introduces its own set of biases and that use of coarse resolution distorts vertical motions in and around organized convection, with consequences for the moisture field.

Acknowledgment. WRB acknowledges support from Office of Naval Research award N00014-11-1-0617 and National Science Foundation award AGS-1253222. AVF acknowledges support from NOAA award NA14OAR4310277. This work was supported in part by the facilities and staff of the Yale University Faculty of Arts and Sciences High Performance Computing Center. We thank Zhiming Kuang and Olivier Pauluis for helpful comments, and Marat Khairoutdinov and Zhiming Kuang for providing the code for SAM.

APPENDIX

Comparison with results of Pauluis et al. (2006)

As stated in the Introduction, Pauluis et al. (2006, hereafter P06) concluded that RAVE enhanced the amplitude of the dry bias that occurs at coarse horizontal resolutions in simulations of radiative-convective equilibrium. We demonstrated the opposite result in this paper and suggest that the difference may arise from the fact that P06 used a much shorter period for their time averages while also increasing their model domain size as resolution was coarsened (holding the number of model grid points constant). Here we present a few relevant model analyses and discuss possible reasons for our contrasting results.

Other studies have shown that larger domains favor the spontaneous aggregation of moist convection and an associated domain-mean drying (e.g. Bretherton et al. 2005; Khairoutdinov and Emanuel 2010), so it seems possible that the domain-mean drying P06 found at coarse resolutions is due to convective aggregation in those correspondingly larger domains. Our 4°-wide domain at 8-km resolution has the same number of grid points as our 1°-wide domain at 2-km resolution, and the former does have a dry bias relative to the latter when 150-day time- and horizontal-means are compared (solid blue line in Fig. 15). This dry bias is about twice as large as those found when resolution is coarsened while holding domain size constant (e.g. Fig. 3). Applying RAVE with $\gamma = 4$ to the 8-km resolution run reduces the dry bias by roughly 30% (relative to the same 2-km resolution run without RAVE). From this one would conclude that RAVE moistens the environment even when the number of grid points is held constant as resolution is coarsened, which is opposite to the finding of P06. However, when we average the specific humidity over an 8-day period, starting after the first 8 days of our simulations, RAVE actually enhances the dry bias (compare solid and dashed black lines in Fig. 15). One might speculate that RAVE speeds up the convective self-aggregation that is associated with the domain mean drying while moistening the final aggregated state, but further analysis would be needed to draw a firm conclusion.

Other differences between the model configurations used here and by P06 might also contribute to our contrasting results. P06 imposed vertical wind shear in their models by relaxing horizontal winds to either a weak or strong shear profile (our simulations did not use imposed shear). They noted that strong shear produces organized convection, consistent with previous studies showing that shear can cause convection to arrange into bands or arcs (e.g. Robe and Emanuel 2001). Vertical wind shear can also inhibit the self-aggregation of convection into a single cluster (e.g.

Tompkins 2001), although Bretherton et al. (2005) applied the same magnitude of shear used in the "weak shear" simulations of P06 and found that it slowed but did not halt the self-aggregation process. The implications of this slowing for integrations that only last 16 days are unclear. This study and P06 also used models with different parameterizations of microphysics and radiation, which might influence the character of any organization or whether aggregation occurs. Thus, it is not possible to definitively determine the reasons for our different results, but this appendix has presented some evidence in support of the hypothesis that the difference is primarily caused by the use in P06 of a short averaging period and a methodology that enlarged domain size as resolution was coarsened.

References

Arakawa, A., 2004: The cumulus parameterization problem: Past, present, and future. *J. Climate*, **17 (13)**, 2493–2525.

Bell, R., J. Strachan, P. L. Vidale, K. Hodges, and M. Roberts, 2013: Response of Tropical Cyclones to Idealized Climate Change Experiments in a Global High-Resolution Coupled General Circulation Model. *Journal of Climate*, **26 (20)**, 7966–7980, doi:10.1175/jcli-d-12-00749.1.

Bender, M. A., T. R. Knutson, R. E. Tuleya, J. J. Sirutis, G. A. Vecchi, S. T. Garner, and I. M. Held, 2010: Modeled impact of anthropogenic warming on the frequency of intense atlantic hurricanes. *Science*, **327 (5964)**, 454–458.

Bister, M., and K. A. Emanuel, 1997: The genesis of Hurricane Guillermo: TEXMEX analyses and a modeling study. *Monthly Weather Review*, **125 (10)**, 2662–2682.

Boos, W., and Z. Kuang, 2010: Mechanisms of poleward-propagating, intraseasonal convective anomalies in cloud-system resolving models. *in press at J. Atmos. Sci.*

Bretherton, C., P. Blossey, and M. Khairoutdinov, 2005: An energy-balance analysis of deep convective self-aggregation above uniform SST. *J. Atmos. Sci.*, **62 (12)**, 4273–4292.

Bretherton, C. S., and P. K. Smolarkiewicz, 1989: Gravity waves, compensating subsidence and detrainment around cumulus clouds. *Journal of the Atmospheric Sciences*, **46 (6)**, 740–759.

Browning, G., and H.-O. Kreiss, 1986: Scaling and computation of smooth atmospheric motions. *Tellus A*, **38 (4)**, 295–313.

Camargo, S. J., 2013: Global and Regional Aspects of Tropical Cyclone Activity in the CMIP5 Models. *Journal of Climate*, **26 (24)**.

Chavas, D. R., and K. Emanuel, 2014: Equilibrium tropical cyclone size in an idealized state of axisymmetric radiative–convective equilibrium*. *Journal of the Atmospheric Sciences*, **71 (5)**, 1663–1680.

Cohen, B. G., and G. C. Craig, 2004: The response time of a convective cloud ensemble to a change in forcing. *Q. J. R. Meteorol. Soc.*, **130 (598)**, 933–944.

Emanuel, K., J. Callaghan, and P. Otto, 2008: A Hypothesis for the Redevelopment of Warm-Core Cyclones over Northern Australia*. *Monthly Weather Review*, **136 (10)**, 3863–3872.

Emanuel, K., and D. Nolan, 2004: Tropical cyclone activity and the global climate system. *26th Conf. on Hurricanes and Tropical Meteorology*, Miami, FL, American Meteorological Society.

Emanuel, K., A. A. Wing, and E. M. Vincent, 2013: Radiative-convective instability. *Journal of Advances in Modeling Earth Systems*, **6**, 75–90.

Emanuel, K. A., 1988: The maximum intensity of hurricanes. *Journal of the Atmospheric Sciences*, **45 (7)**, 1143–1155.

Emanuel, K. A., 1989: The finite-amplitude nature of tropical cyclogenesis. *Journal of the Atmospheric Sciences*, **46 (22)**, 3431–3456.

Emanuel, K. A., 1995: On thermally direct circulations in moist atmospheres. *J. Atmos. Sci.*, **52**, 1529–1536.

Fedorov, A. V., C. M. Brierley, and K. Emanuel, 2010: Tropical cyclones and permanent El Nino in the early Pliocene epoch. *Nature*, **463 (7284)**, 1066–1070.

Fierro, A. O., R. F. Rogers, F. D. Marks, and D. S. Nolan, 2009: The impact of horizontal grid spacing on the microphysical and kinematic structures of strong tropical cyclones simulated with the WRF-ARW model. *Monthly Weather Review*, **137 (11)**.

Frisius, T., 2006: Surface-flux-induced tropical cyclogenesis within an axisymmetric atmospheric balanced model. *Quarterly Journal of the Royal Meteorological Society*, **132 (621)**, 2603–2623.

Garner, S., D. Frierson, I. Held, O. Pauluis, and G. Vallis, 2007: Resolving convection in a global hypohydrostatic model. *J. Atmos. Sci.*, **64**, 2061–2075.

Gentry, M. S., and G. M. Lackmann, 2010: Sensitivity of simulated tropical cyclone structure and intensity to horizontal resolution. *Monthly Weather Review*, **138 (3)**.

Gualdi, S., E. Scoccimarro, and A. Navarra, 2008: Changes in Tropical Cyclone Activity due to Global Warming: Results from a High-Resolution Coupled General Circulation Model. *Journal of Climate*, **21 (20)**, 5204–5228, doi:10.1175/2008jcli1921.1.

Hendricks, E. A., M. T. Montgomery, and C. A. Davis, 2004: The role of "vortical" hot towers in the formation of tropical cyclone Diana (1984). *J. Atmos. Sci.*, **61 (11)**, 1209–1232.

Houze, R. A., 1993: *Cloud dynamics*. Academic Press, San Diego, California, 573 pp.

Khairoutdinov, M., and K. Emanuel, 2010: Aggregated Convection and the Regulation of Tropical Climate. *29th Conference on Hurricanes and Tropical Meteorology*, Tucson, AZ, American Meteorological Society.

Khairoutdinov, M., and D. Randall, 2003: Cloud resolving modeling of the ARM summer 1997 IOP: Model formulation, results, uncertainties, and sensitivities. *J. Atmos. Sci.*, **60 (4)**, 607–625.

Kiehl, J., J. Hack, G. Bonan, B. Boville, D. Williamson, and P. Rasch, 1998: The National Center for Atmospheric Research Community Climate Model: CCM3*. *J. Climate*, **11 (6)**, 1131–1149.

Knutson, T., J. Sirutis, S. Garner, G. Vecchi, and I. Held, 2008: Simulated reduction in Atlantic hurricane frequency under twenty-first-century warming conditions. *Nature Geosci.*, **1 (7)**, 479–479, doi:10.1038/ngeo229.

Knutson, T. R., J. J. Sirutis, S. T. Garner, I. M. Held, and R. E. Tuleya, 2007: Simulation of the recent multidecadal increase of atlantic hurricane activity using an 18-km-grid regional model. *Bulletin of the American Meteorological Society*, **88 (10)**, 1549–1565.

Knutson, T. R., and Coauthors, 2013: Dynamical Downscaling Projections of Twenty-First-Century Atlantic Hurricane Activity: CMIP3 and CMIP5 Model-Based Scenarios. *Journal of Climate*, **26 (17)**.

Kuang, Z., P. N. Blossey, and C. S. Bretherton, 2005: A new approach for 3D cloud resolving simulations of large scale atmospheric circulation. *Geophys. Res. Lett.*, **32**, L02 809, doi:10.1029/2004GL021024.

Lane, T. P., and J. C. Knievel, 2005: Some effects of model resolution on simulated gravity waves generated by deep, mesoscale convection. *Journal of the atmospheric sciences*, **62 (9)**, 3408–3419.

Lee, J., and A. MacDonald, 2000: QNH: Mesoscale bounded derivative initialization and winter storm test over complex terrain. *Mon. Wea. Rev.*, **128 (4)**, 1037–1051.

Liu, C., and M. W. Moncrieff, 2004: Effects of convectively generated gravity waves and rotation on the organization of convection. *Journal of the Atmospheric Sciences*, **61 (17)**.

Ma, D., W. R. Boos, and Z. Kuang, 2014: Effects of orography and surface heat fluxes on the South Asian Summer Monsoon. *Journal of Climate*, in press.

MacDonald, A., J. Lee, and S. Sun, 2000a: QNH: Design and test of a quasi-nonhydrostatic model for mesoscale weather prediction. *Mon. Wea. Rev.*, **128 (4)**, 1016–1036.

MacDonald, A., J. Lee, and Y. Xie, 2000b: The use of quasi-nonhydrostatic models for mesoscale weather prediction. *J. Atmos. Sci.*, **57 (15)**, 2493–2517.

Manabe, S., J. L. Holloway Jr, and H. M. Stone, 1970: Tropical circulation in a time-integration of a global model of the atmosphere. *Journal of the Atmospheric Sciences*, **27 (4)**, 580–613.

Mapes, B. E., 1993: Gregarious tropical convection. *Journal of the Atmospheric Sciences*, **50 (13)**, 2026–2037.

McBride, J. L., 1984: Comments on "simulation of hurricane-type vortices in a general circulation model". *Tellus A*, **36 (1)**, 92–93.

Merlis, T. M., M. Zhao, and I. M. Held, 2013: The sensitivity of hurricane frequency to ITCZ changes and radiatively forced warming in aquaplanet simulations. *Geophysical Research Letters*, **40 (15)**, 4109–4114.

Moeng, C.-H., M. A. LeMone, M. F. Khairoutdinov, S. K. Krueger, P. A. Bogenschutz, and D. A. Randall, 2009: The tropical marine boundary layer under a deep convection system: a large-eddy simulation study. *Journal of Advances in Modeling Earth Systems*, **1 (4)**.

Muller, C. J., and I. M. Held, 2012: Detailed investigation of the self-aggregation of convection in cloud-resolving simulations. *Journal of the Atmospheric Sciences*, **69 (8)**.

Murakami, H., and M. Sugi, 2010: Effect of model resolution on tropical cyclone climate projections. *Sola*, **6 (0)**, 73–76.

Nicholls, M. E., R. A. Pielke, and W. R. Cotton, 1991: Thermally forced gravity waves in an atmosphere at rest. *Journal of the Atmospheric Sciences*, **48 (16)**, 1869–1884.

Pauluis, O., D. Frierson, S. Garner, I. Held, and G. Vallis, 2006: The hypohydrostatic rescaling and its impacts on modeling of atmospheric convection. *Theor. Comput. Fluid Dyn.*, **20 (5)**, 485–499.

Pauluis, O., and S. Garner, 2006: Sensitivity of radiative–convective equilibrium simulations to horizontal resolution. *Journal of the Atmospheric Sciences*, **63 (7)**, 1910–1923.

Raymond, D., S. Sessions, and Z. Fuchs, 2007: A theory for the spinup of tropical depressions. *Q. J. R. Meteorol. Soc.*, **133**, 1743–1754.

Robe, F. R., and K. A. Emanuel, 2001: The effect of vertical wind shear on radiative-convective equilibrium states. *J. Atmos. Sci.*, **58 (11)**, 1427–1445.

Scoccimarro, E., and Coauthors, 2011: Effects of Tropical Cyclones on Ocean Heat Transport in a High-Resolution Coupled General Circulation Model. *Journal of Climate*, **24 (16)**, 4368–4384, doi:10.1175/2011jcli4104.1.

Skamarock, W. C., and J. B. Klemp, 1994: Efficiency and accuracy of the Klemp-Wilhelmson time-splitting technique. *Mon. Wea. Rev.*, **122 (11)**, 2623–2630.

Strachan, J., P. L. Vidale, K. Hodges, M. Roberts, and M.-E. Demory, 2013: Investigating Global Tropical Cyclone Activity with a Hierarchy of AGCMs: The Role of Model Resolution. *Journal of Climate*, **26 (1)**, 133–152, doi:10.1175/jcli-d-12-00012.1.

Sun, Y., L. Yi, Z. Zhong, Y. Hu, and Y. Ha, 2013: Dependence of model convergence on horizontal resolution and convective parameterization in simulations of a tropical cyclone at gray-zone resolutions. *Journal of Geophysical Research: Atmospheres*, **118 (14)**, 7715–7732.

Tompkins, A. M., 2001: Organization of tropical convection in low vertical wind shears: The role of water vapor. *J. Atmos. Sci.*, **58 (6)**, 529–545.

Villarini, G., and G. A. Vecchi, 2012: Twenty-first-century projections of North Atlantic tropical storms from CMIP5 models. *Nature Climate Change*, **2 (8)**, 604–607.

Vitart, F., J. Anderson, and W. Stern, 1997: Simulation of interannual variability of tropical storm frequency in an ensemble of gcm integrations. *Journal of Climate*, **10 (4)**, 745–760.

Walsh, K., S. Lavender, E. Scoccimarro, and H. Murakami, 2013: Resolution dependence of tropical cyclone formation in CMIP3 and finer resolution models. *Climate dynamics*, **40 (3-4)**, 585–599.

Wing, A. A., and K. A. Emanuel, 2013: Physical mechanisms controlling self-aggregation of convection in idealized numerical modeling simulations. *Journal of Advances in Modeling Earth Systems*, **6**, 59–74.

Wu, L., and Coauthors, 2014: Simulations of the present and late 21st century western North Pacific tropical cyclone activity using a regional model. *Journal of Climate*, in press.

Zarzycki, C. M., and C. Jablonowski, 2014: A multidecadal simulation of atlantic tropical cyclones using a variable-resolution global atmospheric general circulation model. *Journal of Advances in Modeling Earth Systems*, **6 (3)**, 805–828.

Zhao, M., and I. M. Held, 2010: An Analysis of the Effect of Global Warming on the Intensity of Atlantic Hurricanes Using a GCM with Statistical Refinement. *Journal of Climate*, **23 (23)**.

Zhao, M., I. M. Held, and S.-J. Lin, 2012: Some counterintuitive dependencies of tropical cyclone frequency on parameters in a gcm. *J. Atmos. Sci.*, **69 (7)**, 2272–2283.

Zhao, M., I. M. Held, S.-J. Lin, and G. A. Vecchi, 2009: Simulations of Global Hurricane Climatology Interannual Variability, and Response to Global Warming Using a 50-km Resolution GCM. *Journal of Climate*, **22 (24)**, 6653–6678, doi:10.1175/2009jcli3049.1.

LIST OF FIGURES

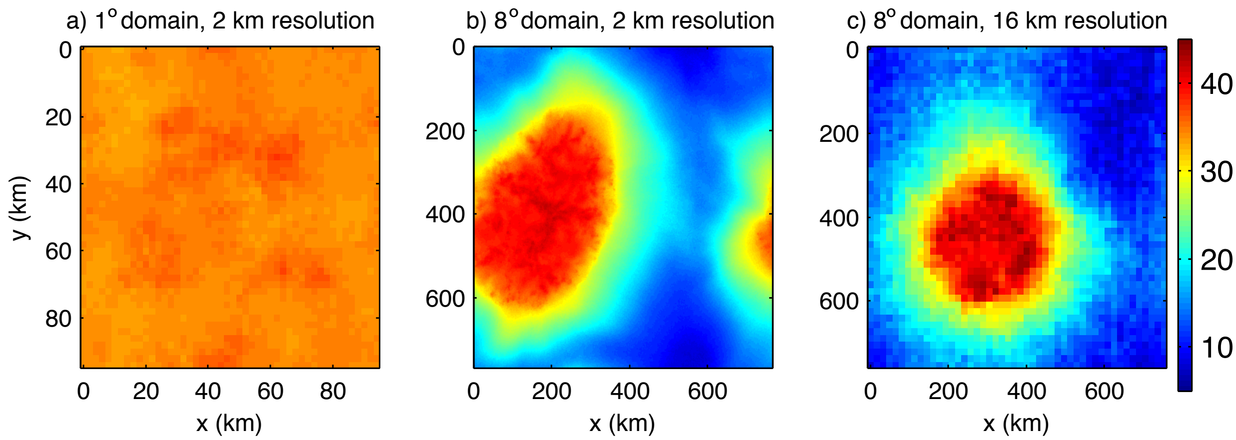

FIG. 1. Precipitable water (mm) in non-rotating domains 50 days after model initialization for different domain sizes and horizontal resolutions, all without RAVE (i.e. $\gamma = 1$). a) The 96 km-wide domain at 2 km resolution, b) the 768 km-wide domain at 2 km resolution, and c) the 768 km-wide domain at 16 km resolution. Note the change in horizontal scale between (a) and (b, c).

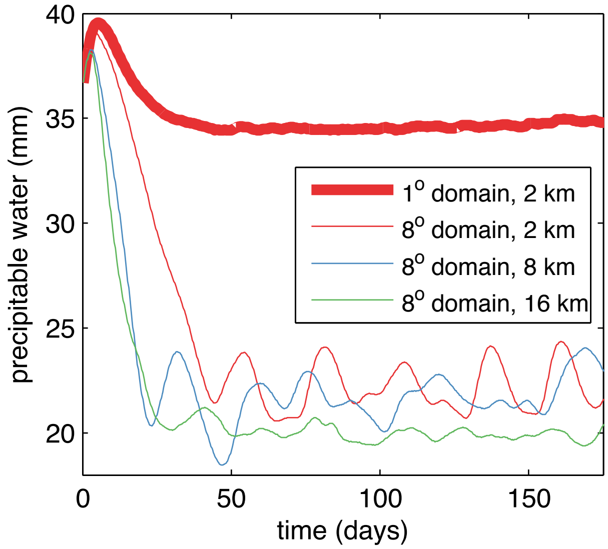

FIG. 2. Time series of horizontally averaged precipitable water for different domain sizes and horizontal resolutions, as shown in the legend, all in non-rotating domains without RAVE (i.e. $\gamma = 1$). In this and subsequent figures, line thickness varies with domain size, line color varies with resolution, and line style (e.g. solid or dashed) varies with RAVE factor.

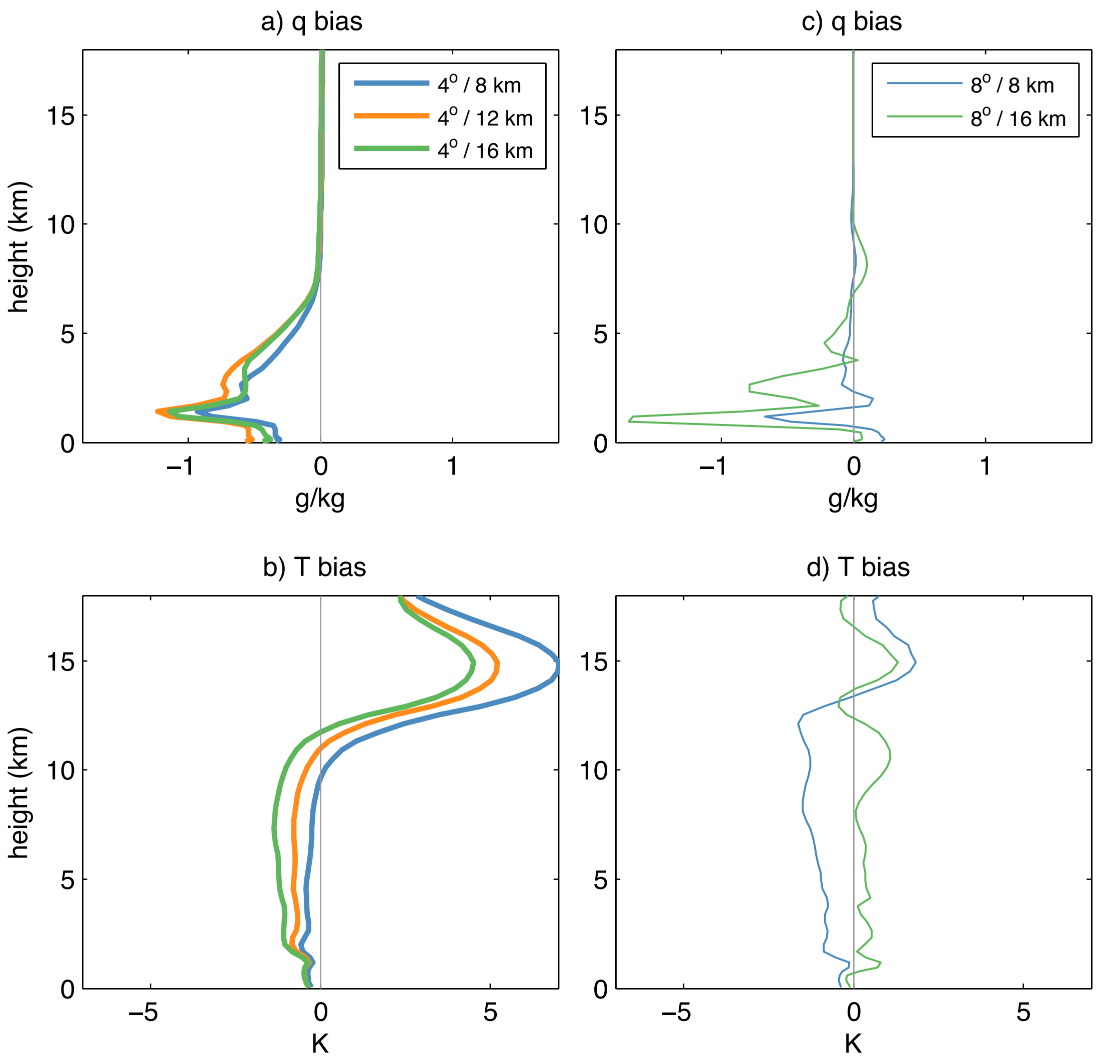

FIG. 3. Time- and horizontal-mean bias, relative to integrations performed at 2 km horizontal resolution, in specific humidity (top panels) and temperature (bottom panels). All quantities are for integrations without RAVE, and were averaged over the last 150 days of integrations lasting 200 days. Line color varies with horizontal resolution as indicated in the legends in the top panels. Left panels show biases in the 4°-wide domain (relative to a 2 km-resolution run in a 4°-wide domain), and right panels show biases in the 8°-wide domain (relative to a 2 km-resolution run in an 8°-wide domain).

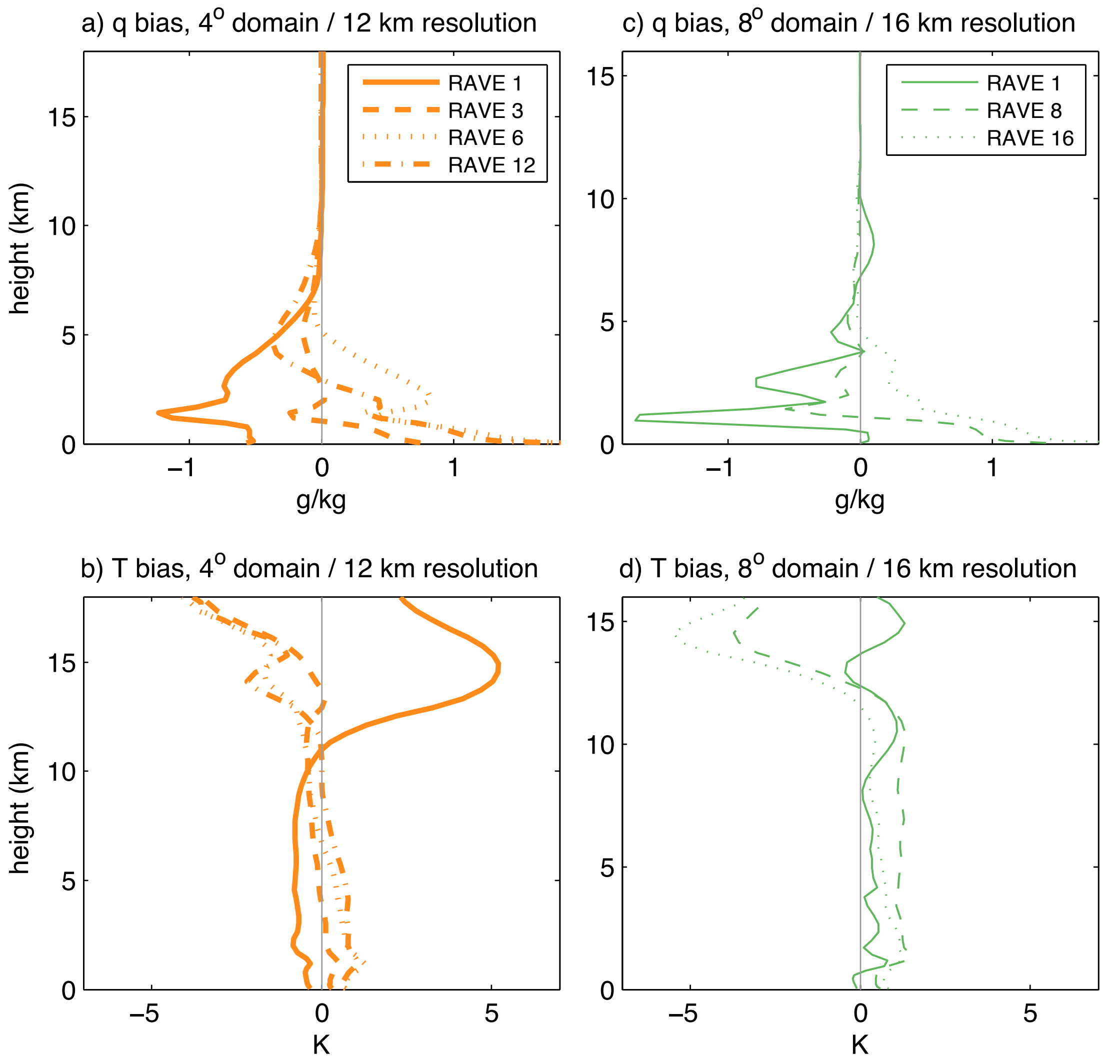

913 FIG. 4. As in Fig. 3 but showing how biases change as the RAVE factor is increased. Left panels show the bias
914 in 12 km-resolution integrations relative to a 2 km-resolution integration without RAVE (i.e. $\gamma = 1$), all in 4°-
915 wide domains. Right panels show bias in 16 km-resolution integrations relative to a 2 km-resolution integration
916 without RAVE, all in 8°-wide domains. Legends in top panels show the values of γ.

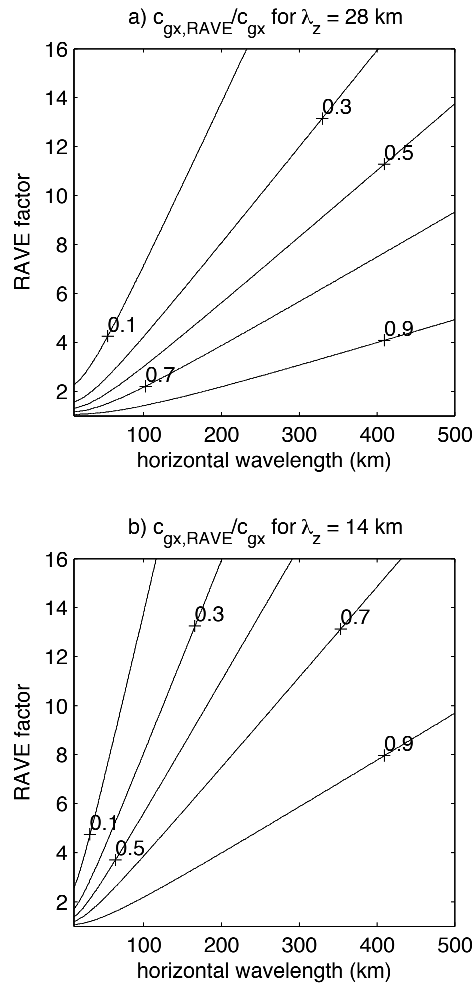

FIG. 5. Coefficient by which RAVE reduces the horizontal group velocity of gravity waves with vertical wavelengths of a) 28 km and b) 14 km.

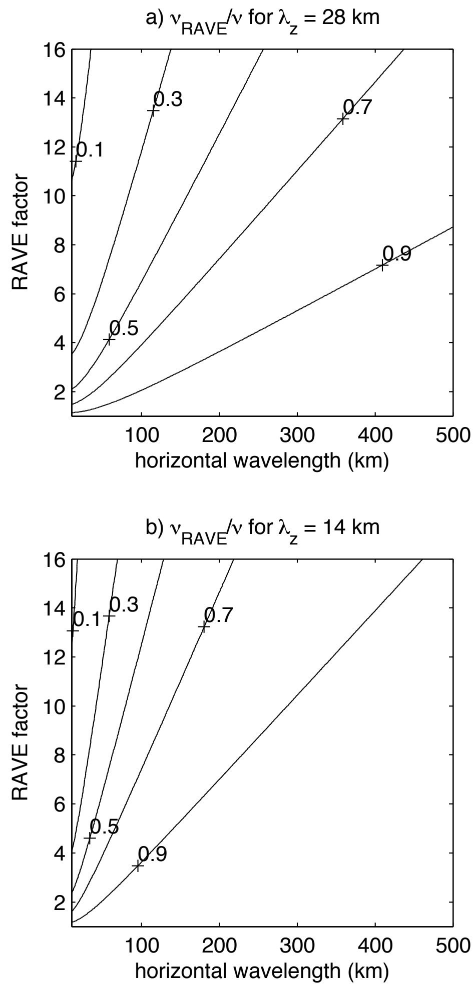

FIG. 6. Coefficient by which RAVE reduces the frequency (and thus the amplitude) of gravity waves with vertical wavelengths of a) 28 km and b) 14 km.

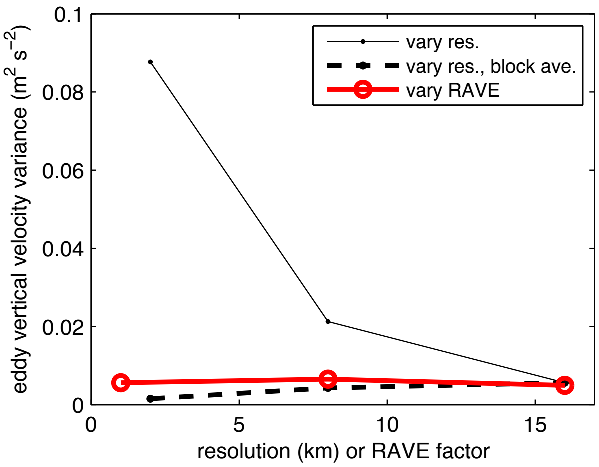

FIG. 7. Eddy vertical velocity variance at 1 km altitude in 8°-wide non-rotating domains for various resolutions without RAVE (black lines) and for various RAVE factors at 16 km resolution (red line). Thin solid black line shows results when all calculations are performed at the native model resolution, while thick dashed black line shows results when vertical velocity was block-averaged to a 16 $\times$ 16 km grid before analysis. Eddies are defined as deviations from the time- and horizontal-mean, and all quantities are evaluated over 150 days.

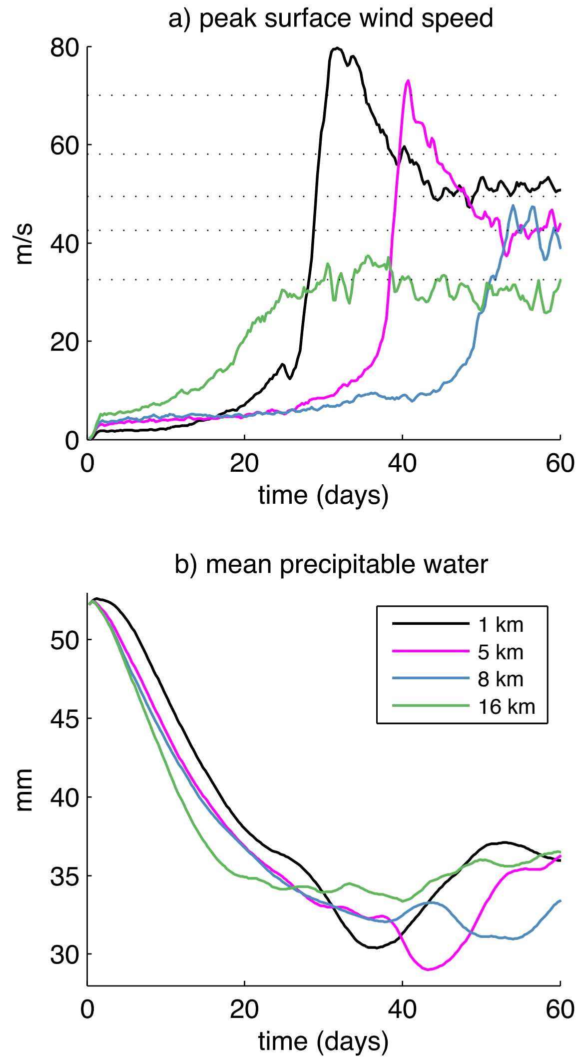

926 FIG. 8. Example time series of a) maximum surface wind speed and b) domain-mean precipitable water at different horizontal resolutions in rotating domains. All are for runs conducted on an f-plane at 20°N with a domain width of 1200 km). Horizontal dotted lines in (a) mark lower bounds of the five Saffir-Simpson intensity categories.

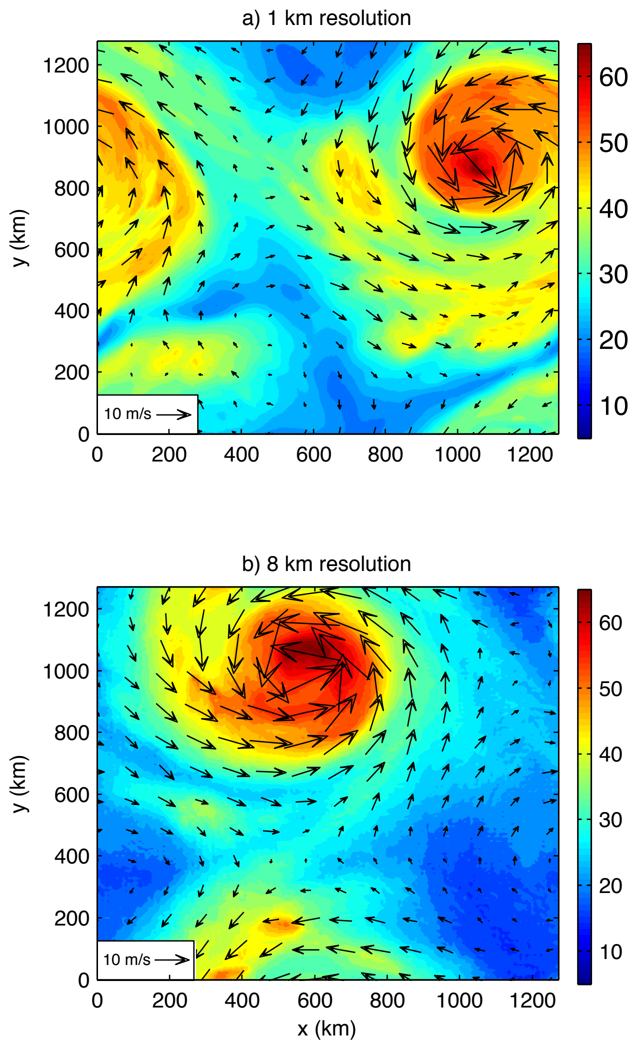

FIG. 9. Precipitable water (mm, color shading) and surface winds (vectors) in rotating domains for different horizontal resolutions, all without RAVE ($\gamma = 1$) on the day when the tropical cyclone first achieves Saffir-Simpson category 1. Top panel is for 1 km horizontal resolution and bottom panel for 8 km resolution.

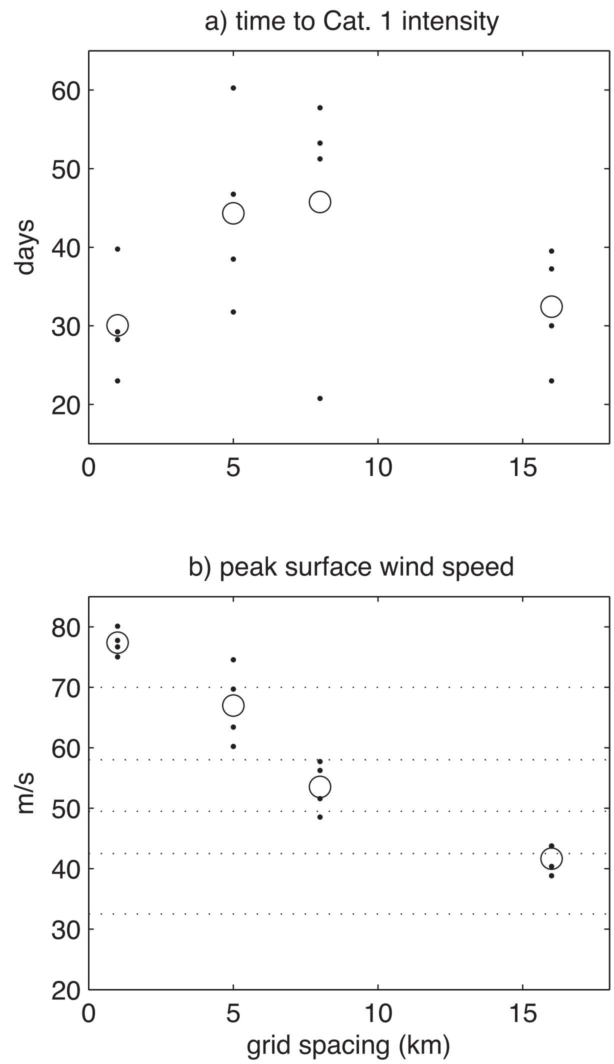

FIG. 10. Metrics of tropical cyclogenesis for ensembles of integrations conducted in rotating domains at different horizontal resolutions, all without RAVE ($\gamma = 1$) and with domain widths of 1200 km. a) Time between model initialization and the day on which the TC achieves Saffir-Simpson category 1 intensity. b) Maximum 6-hourly averaged surface wind speed during the entire simulation. Small black dots show values for individual ensemble members, and open circles show the ensemble mean at a given resolution. Horizontal dotted lines in (b) mark lower bounds of the five Saffir-Simpson intensity categories.

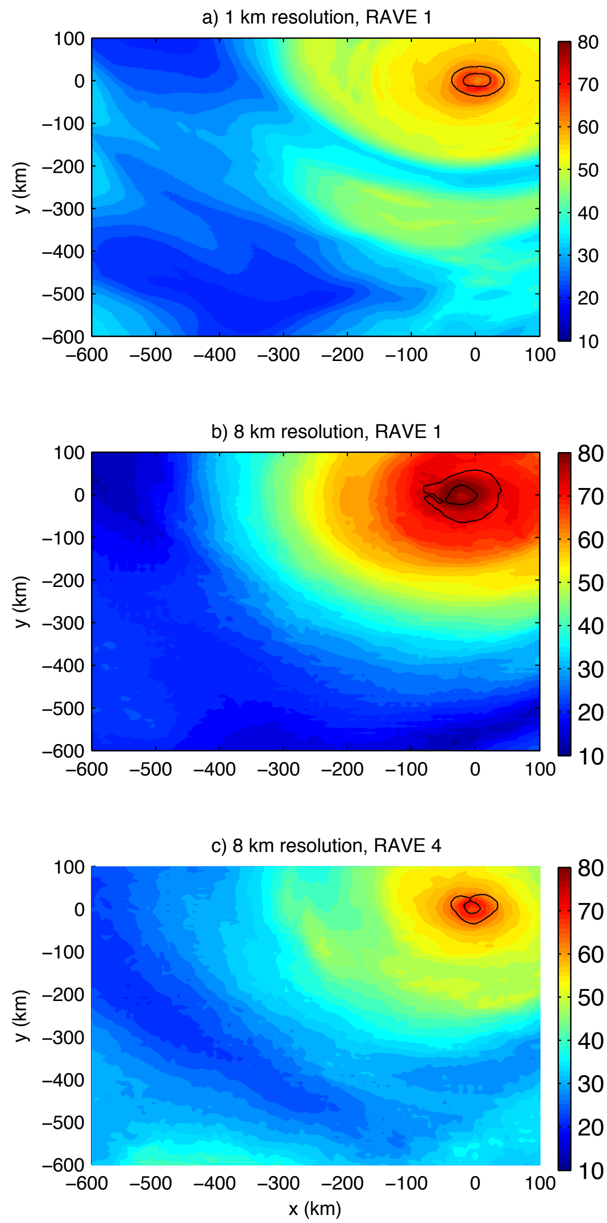

FIG. 11. Precipitable water (mm, color shading) and the 35 m s^{-1} surface isotach in rotating domains for different horizontal resolutions on the day when the tropical cyclone first achieves Saffir-Simpson category 2. a) For 1 km resolution without RAVE, b) for 8 km horizontal resolution without RAVE, and c) for 8 km resolution with $\gamma = 4$.

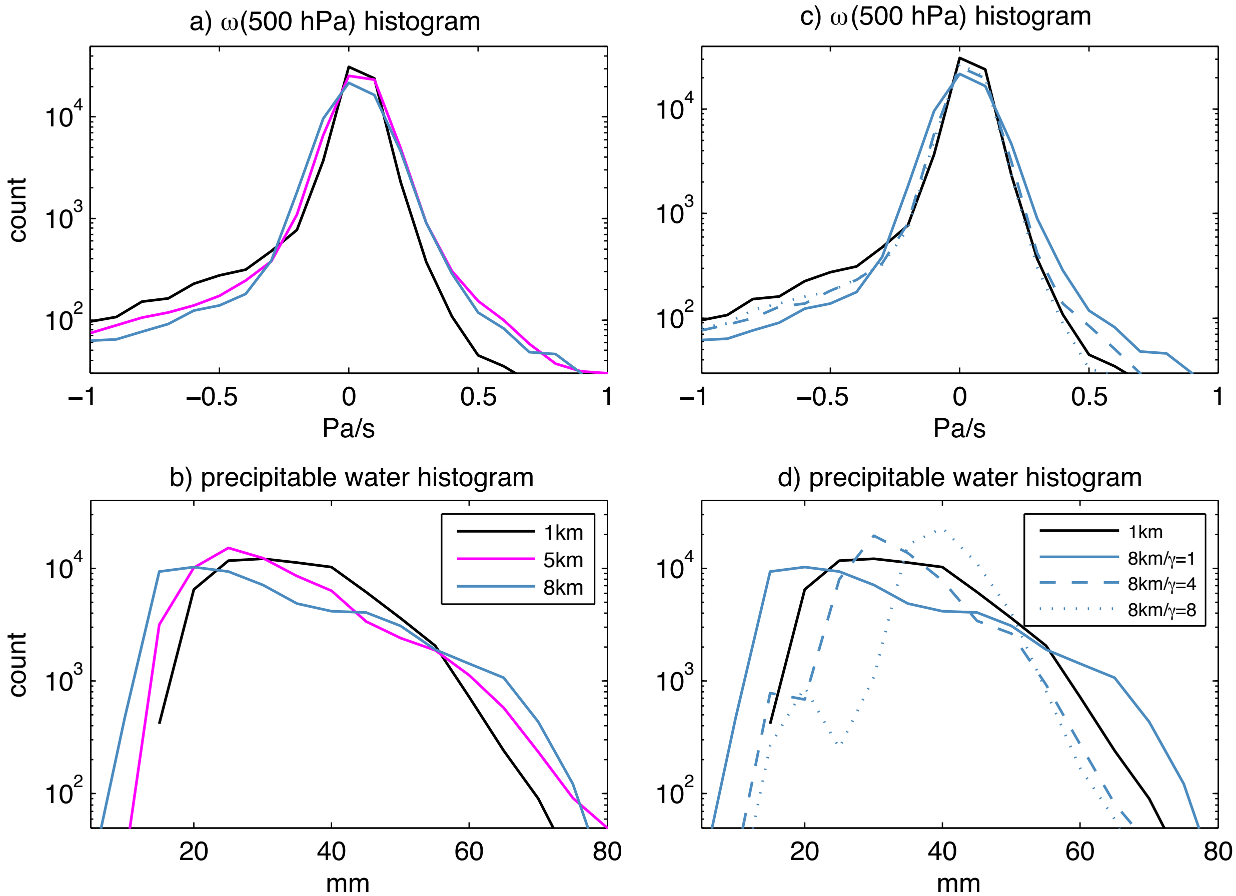

FIG. 12. Histograms of vertical pressure velocity (top panels) and precipitable water (bottom bottom panels) in simulations with rotation for the 2 days after the tropical cyclone achieves category 1 intensity. Left panels show results without RAVE for different horizontal resolutions shown in the legend of (b). Right column shows results for 1 km resolution without RAVE and for 8 km resolution with different RAVE factors as shown in the legend in (d). Results for the 1 km- and 8 km-resolution integrations without RAVE are repeated in all panels to ease comparison.

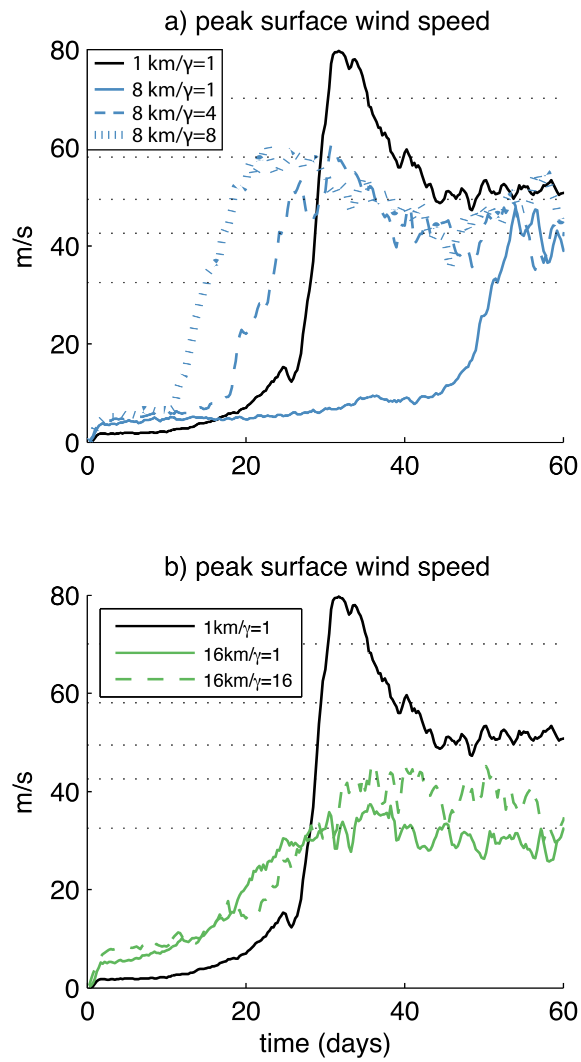

FIG. 13. As in Fig. 8a but for varying RAVE factor at a) 8 km resolution and b) 16 km resolutions. The result for 1 km resolution without RAVE is repeated in both panels for reference.

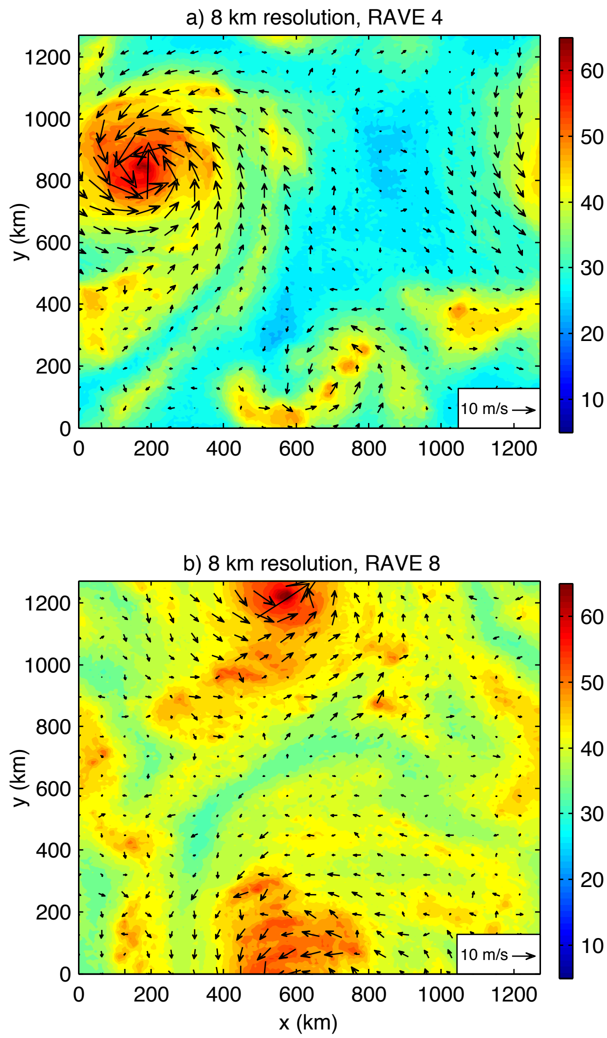

FIG. 14. As in Fig. 9 but for 8 km horizontal resolution with a) $\gamma = 4$ and b) $\gamma = 8$.

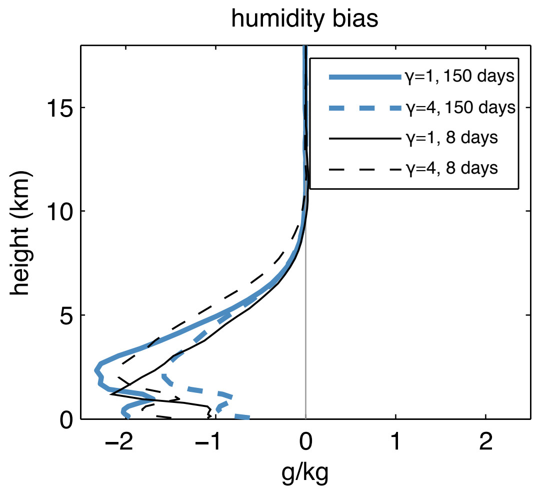

FIG. 15. Time- and horizontal-mean difference in specific humidity between integrations conducted at 8 km resolution and 2 km resolution with the same number of grid points (the 8 km resolution run is thus conducted in a 4°-wide domain, and the 2 km resolution run in a 1°-wide domain). Solid lines denote results without RAVE and dashed lines with a RAVE factor of 4 for the 8-km resolution runs. RAVE was not applied in the 2-km resolution run that was used as the control. Thicker blue lines show results averaged over the last 150 days of the 200-day integration, and thinner black lines show results averaged over 8 days starting on day 9.